University of Sunderland

Oladapo, Bankole, Ismail, Sikiru, Ikumapayi, Omolayo and Karagiannidis, Panagiotis (2022) Impact of rGO-coated PEEK and lattice on bone implant. Colloids and Surfaces B: Biointerfaces.

Impact of rGO-coated PEEK and lattice on bone implant

Bankole I. Oladapo [a,b,*], Sikiru O. Ismail [c], Omolayo M. Ikumapayi [d], Panagiotis G. Karagiannidis [a]

[a] *School of Engineering, Faculty of Technology, University of Sunderland, UK*
[b] *Sustainable Development, De Montfort University Leicester, UK*
[c] *Centre for Engineering Research, Department of Engineering, University of Hertfordshire, UK*
[d] *Department of Mechanical and Mechatronics Engineering, Afe Babalola University, Ado-Ekiti, Nigeria*

ARTICLE INFO

ABSTRACT

The composite coating can effectively inhibit bacterial proliferation and promote the expression of bone-building genes in-vitro. Therefore, a novel production was used to produce poly-ether-ether-ketone, and reduced graphene oxide (PEEK-rGO) scaffolds with ratios of 1–3%, combining a different lattice for a bone implant. An inexpensive method was developed to prepare the new coatings on the PEEK scaffold with reduced graphene oxide (rGO). Mechanical testing, data analysis and cell culture tests for in-vitro biocompatibility scaffold characterisation for the PEEK composite were conducted. Novel computation microanalysis of four-dimensional (4D) printing of microstructure of PEEK-rGO concerning the grain size and three dimensional (3D) morphology was influenced by furrow segmentation of grains cell growth on the composite, which was reduced from an average of 216–155 grains and increased to 253 grains on the last day. The proposed spherical nanoparticles cell grew with time after dispersed PEEK nanoparticles in calcium hydroxyapatite (cHAp) grains. Also, the mechanical tests were carried out to validate the strength of the new composites and compare them to that of a natural bone. The established 3D-printed PEEK composite scaffolds significantly exhibited the potential of bone implants for biomimetic heterogeneous bone repair.

1. Introduction

Fused deposition modelling (FDM) builds a prototype by applying extruded polymer on a table when moving vertically. The polymer feeds in a heated wire in fillets of a semi-liquid or pasty state [1–3]. The movement of the table causes the layer of the piece to be formed, arranging the nets in parallel. Its support is constructed and removed with object construction. A wide range of materials is currently available to develop prototypes in this process. Polyaryletherketones (PAEK) are a group of high-temperature thermoplastic polymers [4–6]. The most widely used polymer is poly-ether-ether-ketone (PEEK), which is often used as a biomedical material in bone grafts.

When the oxygen content of graphene oxide (GO) is reduced by chemical, thermal, or other methods to a lower level, the material is known as reduced graphene oxide (rGO). On the other hand, graphite oxide (GO) is a material formed by oxidising graphite, which results in increased interlayer spacing and functionalisation of the graphite basal planes. Even though graphene is generated by physically exfoliating graphite, its derivatives, such as graphene oxide (GO), a highly reactive form of graphene, and reduced graphene oxide (rGO), produced by chemical or thermal reduction of GO, have distinct characteristics [7–10]. Because of the great biocompatibility of graphene derivatives, they may be used in various biological applications. rGO has been widely utilised to make composites with a range of materials, including metals and metal oxides, to improve supercapacitor performance in various ways, including increasing their capacity. Because graphene and its derivatives have been shown to stimulate cellular adhesion, proliferation, and migration, they have the potential to be used as scaffold materials in tissue engineering applications such as tissue engineering scaffolds. The structural faults of rGO, in contrast to the structural deficiencies in GO, allow it to interact more readily with biomolecules, cells, and polymers. Changing the C/O ratio in a controlled way can also be used to control the electrical conductivity and hydrophilicity of rGO, which are important for controlling many biological processes[11–14].

Therefore, a convenient, fast and inexpensive method to prepare universal coatings on PEEK substrates can be developed. In particular,
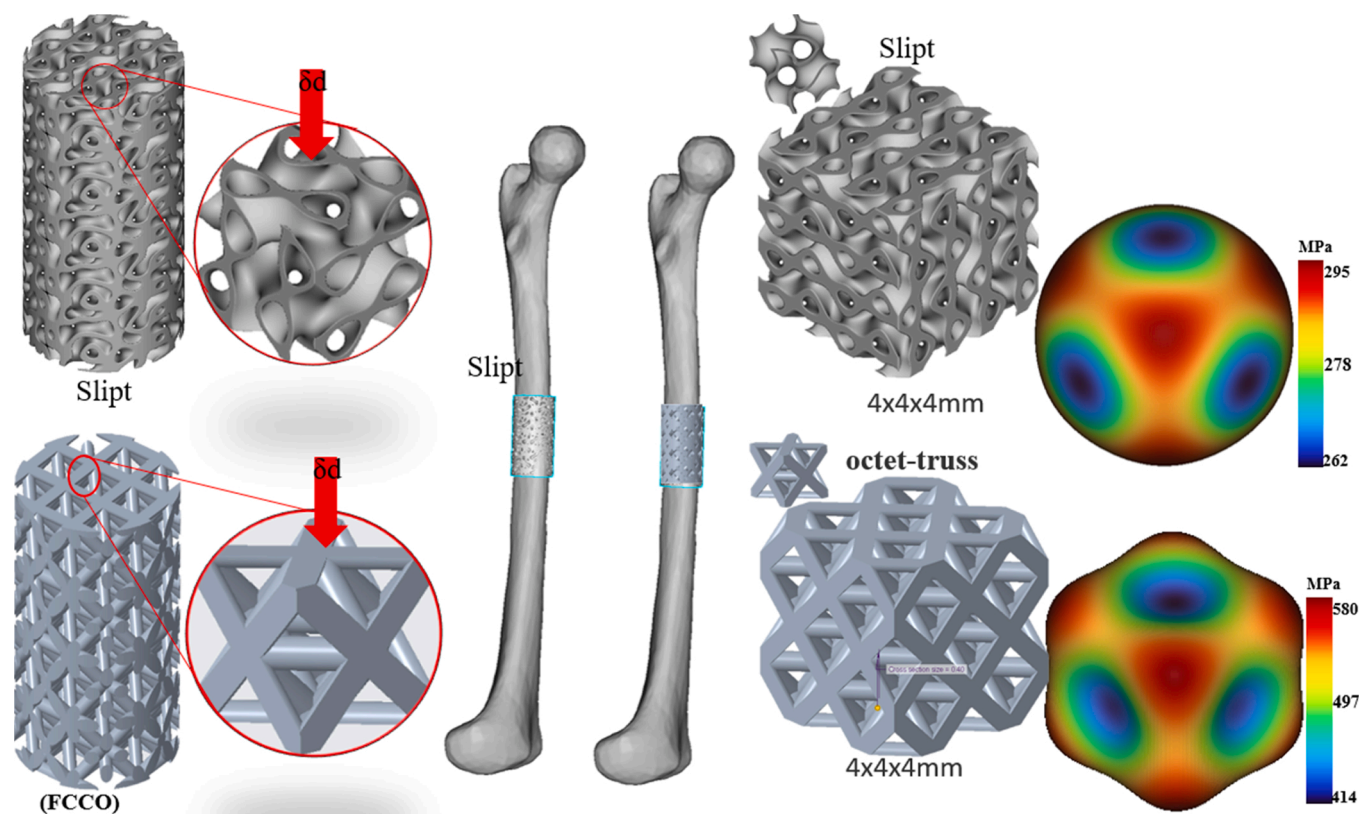

Fig. 1. Lattice design of slipt and face centre cubic-octahedron (FCCO)/octet-truss on the femur bone, as an implant and the corresponding $4 \times 4 \times 4$ mm with the homogenisation of the unit cell of PEEK for biomedical scaffolds tissue engineering generation.

Table 1

Composite compositions in a volume of PEEK-rGO of different densities at 1310 kg/m^3 of PEEK density.

PEEK (wt%)	rGO (wt%)	Young modulus (E) GPa	Poisson ratio (ϑ)	Density (ρ̇) kg/m3	Modulus of rigidity (G) (Gpa)
99.0	1.0	13.8115	0.2256	1316.45	5.6348
98.0	2.0	23.773	0.2013	1322.9	9.8945
97.0	3.0	33.7345	0.1917	1329.4	14.154

reduced graphene oxide (rGO) is continuously modified on PEEK substrates after rGO coating. The composite coating can effectively inhibit bacterial proliferation and promote the expression of bone-building genes in-vitro of poly (ether ether ketone)-reduced graphene oxide (PEEK-rGO) has good bone-building and antibacterial properties [15–17]. FDM three dimensional (3D) printing can provide PEEK-rGO doped compounds with mechanical and biopotential properties suitable for biomedical applications.

Mechanical testing, data analysis, and cell culture tests for in-vitro biocompatibility of scaffold characterisation are important studies required to characterise composite scaffolds [18–20]. Novel computation microanalysis of four-dimensional (4D) printing of scaffold and tailoring the mechanical strength and cell growth of the PEEK-rGO ratio to mimic that of a natural bone of a 3D-printed scaffold are similarly required. Different samples of PEEK composites can be produced to test their properties [21–23]. Pure PEEK can be used as a control in the experiments. The research gaps and novelty are well explained and later illustrated in Fig. 1, which shows a production technique based on the nanostructures porosity analysis that yielded a biomimetic PEEK-rGO composite with an additional control configuration distribution. Precisely, the major contribution of this study is the production of a scaffold with PEEK-rGO with ratios of 1–3%, combining a different lattice with

PEEK and rGO for the bone-implant, as subsequently elucidated.

2. Materials and methods

Medical-grade PEEK filament diameter of 1.75 mm was purchased from VICTREX Corporation, Thornton Cleveleys, UK and Nanjing WeiDa Co. Ltd., Nanjing, China for FDM. Porous PEEK scaffold samples were 3D printed as described in [24–26]. It was prepared via the wet and chemical precipitation method for the coated PEEK scaffold. The suspension was initially stirred in the solution at 400 RPM for 60 min at 60 °C. According to a previous studies [21,27,28]. Besides providing the physical bio-models directly from the biomaterials with high conformity to the virtual bio-models, the scaffolds equipment (3D printer) was constructed with the most varied geometrical dimensions. The study was conducted in the training laboratories at De Montfort University, UK, with industrial support. Scaffold samples were used for surface characterisation, antibacterial tests and in-vitro studies on tissue culture plates. In contrast, PEEK samples were applied for in-vitro drug release and in-vivo animal evaluation [29–31]. First, the PEEK sample was washed three times with acetone and alcohol in an ultrasonic bath for 15 min and rinsed in distilled water, then named nature PEEK. Qingdao Freyr Graphite Company, China supplied the rGO used in this research. Oxidising graphite with permanganate potassium ($KMnO_4$), sulfuric acid (H_2SO_4) and nitric acid (HNO_3) usually depends on the Hummers process. Fig. 1. shows the different production of bone-implant, triply periodic minimal surface (TPMS) lattice structures in FDM 3D printer and 3D-printed polylactic acid (PLA) and PEEK scaffolds of the structure design of slitp and octet-truss before and after adding composite to mimic bone structures, with 50 p to show life representation and dimensions of the scaffolds.

$$\text{Modulus of Elasticity [E] is } \frac{Stress}{Strain} = \frac{\sigma}{\varepsilon}, \text{and} \qquad (1)$$
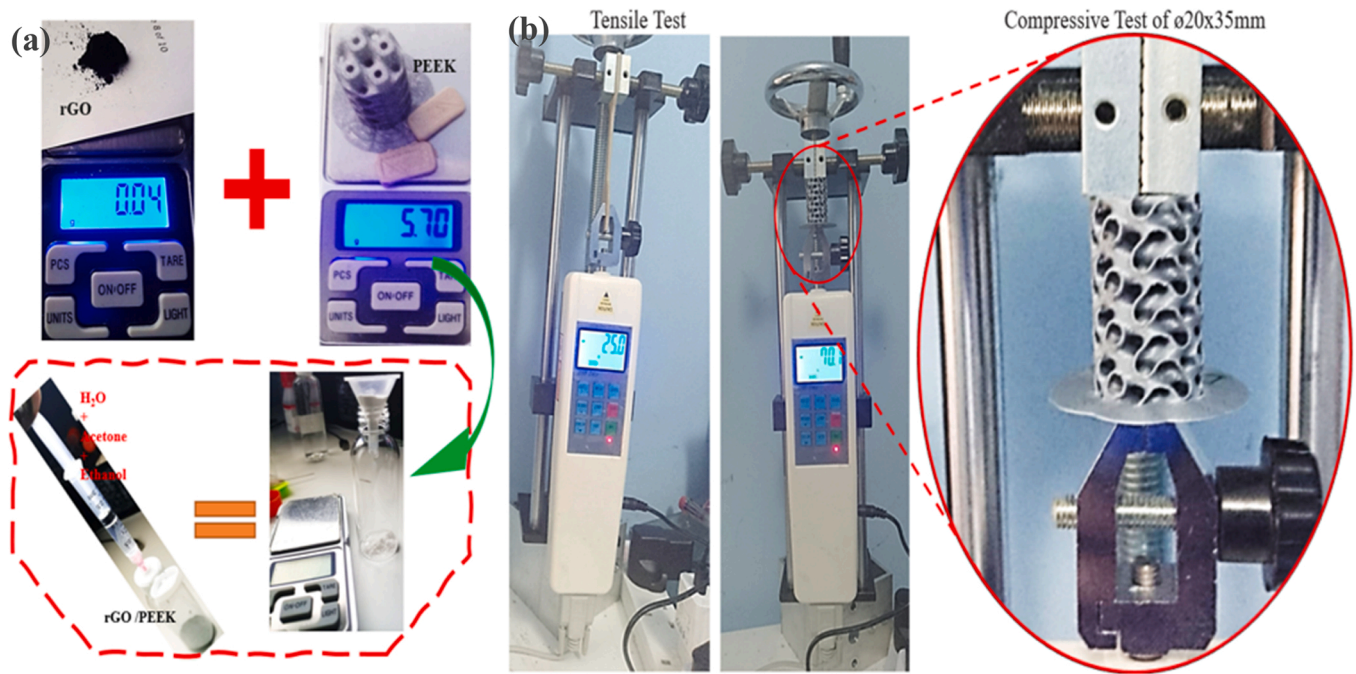
Fig. 2. Fabrications of composite by (a) cold modification of PEEK scaffold and (b) tensile-compressive test set-up and its analysis.
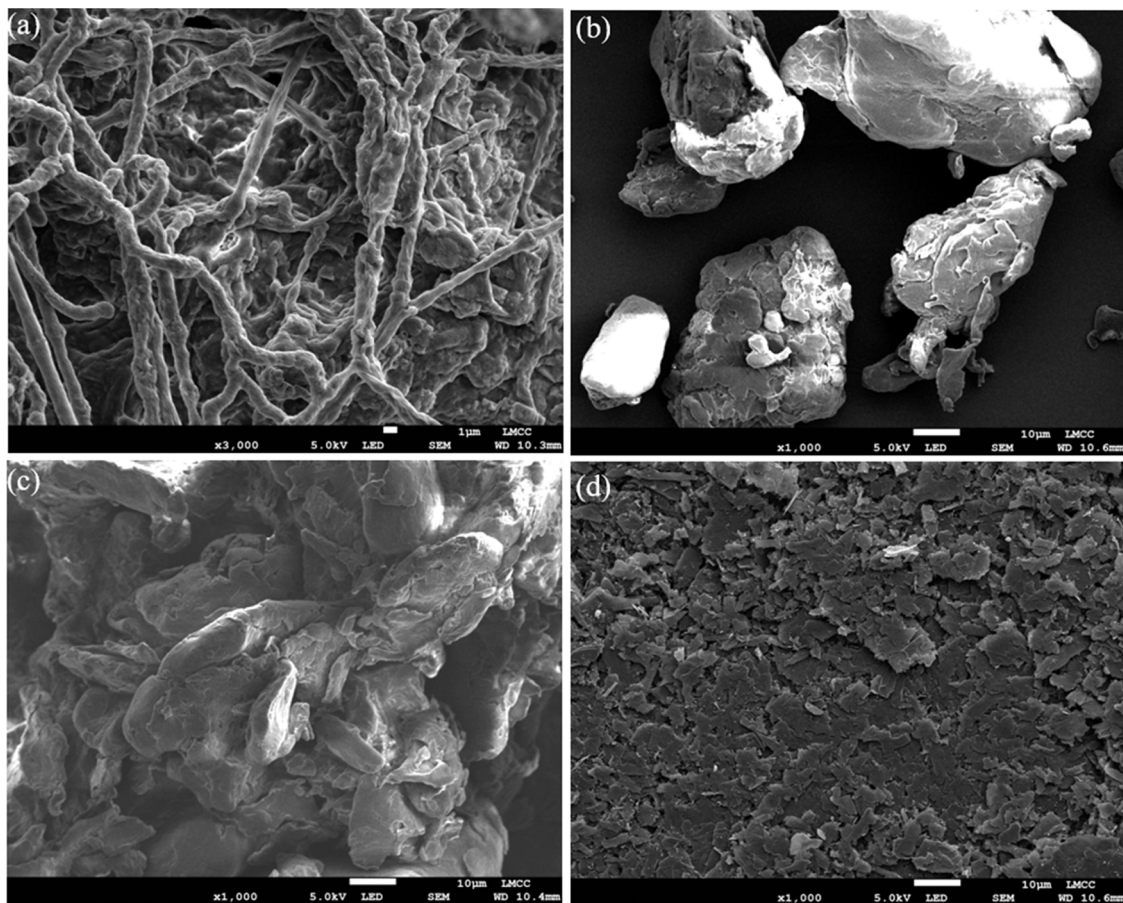

Fig. 3. SEM structures of: (a) PEEK-rGO culture scaffold, (b) PEEK and (c&d) rGO.

Modulus of elasticity

$$E_c = E_p V_p + E_{rGO} V_{rGO}$$

(2)

Modulus of rigidity
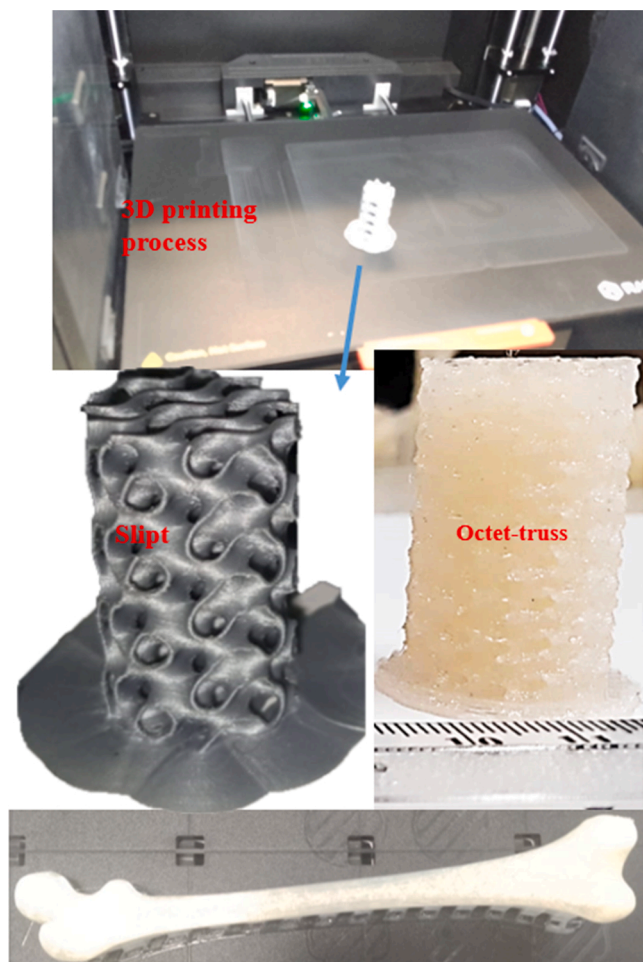
$$G_c = G_p V_p + G_{rGO} V_{rGO}$$

(3)

Fig. 4. Production of bone-implant of slipt and octet-truss TPMS lattice structures in FDM 3D printer to mimic bone structures.

Table 2
Statistics of overall grains - Binarised image after segmentation result of the nanoparticle (Hills detection).

Samples information	24 h		Third day		Seventh-day	
Number of grains	216		155		253	
Total area occupied by the grains (mm^2)	2829 (74.5%)		4112 (81.7%)		4015 (76.1%)	
Density of grains (grains/mm^2)	0.0569		0.0308		0.0479	
Grain parameters	Mean	Std dev	Mean	Std dev	Mean	Std dev
Area (µm^2)	13.10	16.30	26.50	46.50	15.90	20.20
Perimeter (µm)	16.70	9.70	22.90	19.10	18.60	13.00
Equivalent diameter (µm)	3.64	1.86	4.70	3.41	3.87	2.29
Mean diameter (µm)	3.55	1.82	4.55	3.33	3.74	2.21
Min diameter (µm)	2.18	1.33	2.81	2.14	2.26	1.48
Max diameter (µm)	5.48	2.79	7.21	5.44	6.15	3.86
Min diameter angle (deg.)	-9.12	53.90	-29.40	50.10	-18.60	51.40
Max diameter angle (deg.)	-23.30	48.90	-5.94	53.30	-0.32	53.50
Form factor	0.517	0.124	0.494	0.157	0.496	0.142
Aspect ratio	2.78	1.24	3.16	2.70	3.01	1.54
Roundness	0.460	0.118	0.459	0.158	0.430	0.135
Compactness	0.673	0.087	0.666	0.122	0.647	0.104
Orientation (deg.)	78.1	50.2	95.5	54.7	92.2	51.9

Therefore, the modulus of elasticity [E] values for the PEEK, of 3.85GPa, and assuming rGO has 1000 GPa as of a common monolayer of graphene oxide. The most commonly used poison ratio (ϑ) for PEEK is 0.4, from which rGO poison ratio was derived. The density (ρ) of PEEK is 1310 kg/m^3, ρ and ρ of rGO is 1955 kg/m^3. The modulus of rigidity or shear modulus (G) of PEEK, and rGO were 1.375, and 427.350 GPa, respectively, according to Eq. (4) [11,12,33].

$$G = \frac{E}{2(1 - \vartheta)}$$

$$\vartheta_{rGO} = 1 - \frac{E}{2G} = 1 - \frac{1000GP}{2 \times 427.35GP} = 0.17$$

(4)

From Eq. (2), using 99 wt% of PEEK, and 1 wt% of rGO give the expression:

$$E_c = 3.85GPa \; x0.99 + 1000GPax0.01 = 13.8115GPa$$

$$G_c = 1.375GPa \times 0.99 + 427.35GP \times 0.01 = 5.6348$$

2.1. Biocompactivity cell test

The updated Hummers system for natural graphite rGO dispersion was used with H_2SO_4 and $KMnO_4$ as oxidising agents. The substance was washed with hydrochloric acid (HCl) of 5% and then deionised water (diH$_2$O). The implication was exfoliated by 60 min of ultra-sonification, and finally, the rGO scattering was achieved. The rGO-composites were used to obtain epoxy mixtures with an equal epoxy ratio of 70:30 in different percentages by volume of rGO: 0%, 1%, 3% and 5% for 10 min at 25 °C, the composites were mixed, and four different samples were put in an oven at 40 °C [32–34]. The models were retained in the oven for 3.5 h at 40 °C to eliminate the surface moisture.

The rGO reaction with epoxy was completed after 48 h at a room temperature of 25 °C. Table 1 displays the rGO and contents. For in-vitro bioactivity investigations, square scaffolds of 20 x 10 x 5 mm, weighing around 0.60 g, were built vertically and soaked in 25 mL of simulated body fluid (SBF) in glass containers held at 35 °C. About five specimens were tested for each component. SBF was refreshed every day. Ion concentrations in the SBF solution were similar to those in human blood plasma. The specimens were removed from the solution, washed with distilled water, and air-dried after soaking in SBF for 2 or 7 days.

3. Mechanical testing

As previously illustrated in Fig. 1, porosity between 60% and 80% varied among octet-truss and slipt structures with a pore size of 1.0 mm. The pores of the external structure were N1000 µm when the elastic modulus was constant to prevent occlusion of the pores. The interior pores were decrescent to facilitate cell attachment development. Mechanical properties of host bone tissue can be well suited to the same elastic module of different models by regulating the inner and outer strut diameters [35–38]. The pores of the octet-truss system were more significant than the slipt structure porosity. First, the octet-truss structure was chosen, depending on the required range of external pores. The mathematical porosity model and the elastic modulus were used to calculate the corresponding structure porosity according to the need for an elastic modulus value. Finally, in conjunction with the geometrical model of the structure, the corresponding structure calculated geometric parameters and porosity. When the two outer strut parameters were not fit, the outer strut of both structures was determined by that of an inner strut. The octet-truss/FCCO structure was finally generated with a constant elastic modulus. The method used in this innovative study is called homogenisation, which extracts macro-mechanical behaviours from micro-mechanical properties. Fig. 2 depicts the screenshot of the experiments, showing the outcome and result when the compressive test was carried out on different TPMS scaffolds. The general idea was that the micro-mechanical properties were averaged over a chosen
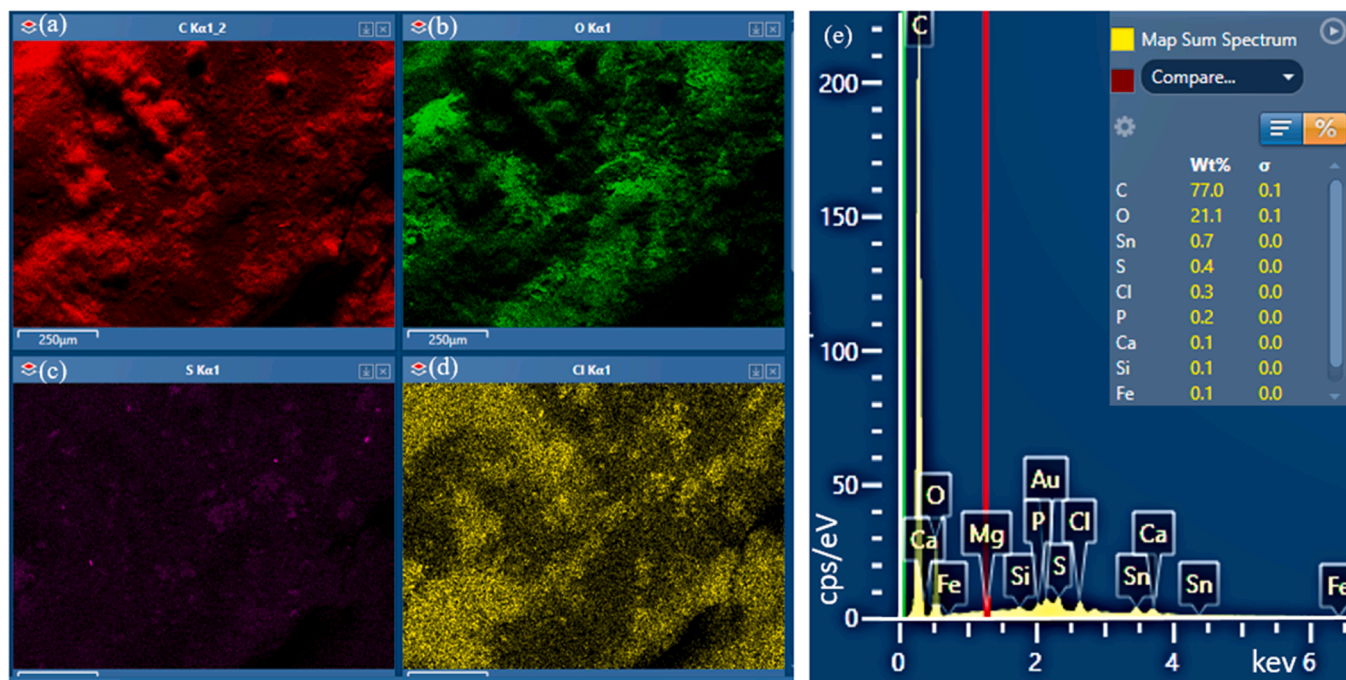
Fig. 5. PEEK-rGO culture scaffold without (a-d), SEM individual element maps, including carbon, oxygen, tin and chlorine of 77%, 21.1%, 0.7% and 0.3%, respectively and (e) composite and the related percentage of the elements extracted from EDS spectrum.

representative volume element. The smallest constituent volume sample of material still represented the whole material. Homogenisation is commonly used with composite materials, but with voids and defects in materials, such as steels. It is essential to know the relationship between micro-mechanical and macro-mechanical properties in all materials.

4. Results and discussion

4.1. Microstructural analysis

Porosity and more effective space forms are another great attraction of these technologies that use particle agglutination to produce scaffolds. The material that makes up the mineral matrix of bones was obtained in powder. The particles did not clump together due to the additive manufacturing (AM) laser beam; the use of the chemical reactions of binder polymer was necessary. Fig. 3 depicts the scanning electron microscope (SEM) structure of the PEEK-rGO culture scaffold with nutrient agar solution (NAS). The microstructure of PEEK, rGO and polymeric binders were awkward to remove either by calcination or solubilisation, particularly in structures with micrometric dimensions that provided resistance to mass transport and thus to the entry and exit of cleaning agents. *In-vitro* studies in simulated body fluid were carried out to analyse the bioactivity of the composites created. Surface alterations were investigated using SEM (Fig. 3). SEM images of all composites indicated a developed layer with flower-like structures and various morphologies, showing an rGO layer and the investigation of the energy dispersive spectroscopy (EDS). As the number of bioglass increased, the surfaces became increasingly porous with lengthy fissures, suggesting a parallel degradation of the formerly smooth surface. Pores and developed fractures were believed to contribute to rGO formation by increasing the rate of ion exchange reactions across the scaffold's mass, which is important for rGO development and the higher bioglass percentage.

4.2. X-ray diffraction

The scaffold used in the InVesalius 3 prototypes is often

biocompatible. It can be used to prepare metal-nylon biocomposites, utilising stainless steel in the powdered form. The X-ray diffraction patterns of the raw powder and composite scaffolds are shown in Fig. 4; the raw PEEK patterns and rGO-resembled those in another research[1, 16,21]. There were only two phases: the PEEK phase and the phase-in powder sintered with AM containing pores diameter of 1000 μm. Fig. 4(a)-(c) are representations of the volume of luminance island of different PEEK-rGO, the continuous wavelet decomposition extract from various percentages nanoparticles, and the analysis of the grain of the binarised microstructure with thresholding of 30% of HAp, respectively. The volumes of the luminance island of different PEEK- were 113, 115, and 217 at a threshold of 112 GL. They meant height surface ratios of 151, 120 and 81.8 GL/mm^2 during the analysis of three days [38–42]. The island means volumes for the three specimens were 107, 532 and 416 GL.mm^2 at a specific decomposition setting of Wavelet Daubechies in ISO 4287 standard (Table 2).

From Fig. 5, the deduced results were as follows: 3D view of square method results with the surface level. Average power spectrum density (PSD) of the dominant spatial frequency of the nanoparticles of PEEK and frequency spectrum of PEEK-HAp particle luminance were obtained at − 33.7, − 48.9 and − 40.8 frequencies. The 3D parameters converted to luminance parameters with ASME B46.1 for maximum height (St) and maximum peak height (Sp) were obtained as 228, 71.9 and 255 GL alongside 156, 29.9 and 170 GL, respectively, according to Fig. 5. The root-mean-square height (Sq) and arithmetic mean height (Sa) were 29.9 and 19.8 GL for the 24 h, 51.9 and 38.5 GL for the third day and 49.2 and 39.3 GL for the seventh day, respectively. The corresponding skewness, Kurtosis and area waviness heights at the Gaussian filter rating of 0.80 mm were 2.36, 10.50 and 219 GL for the 24 h measurements, 1.56, 4.89 and 253 GL for the third day, 0.776 3.220 and 251 GL for the seventh day, respectively. From Fig. 5, using the one corner area-scale method, the number of points was 40 at the smooth-rough crossover (SRC) threshold and a maximum domain scale of 14.5 and 375 mm^2 for the 24 h, 15.1 and 538 mm^2 for the third day and 14.3 and 538 mm^2 for the seventh day. Using the enclosing boxes method in actual units with a fractal dimension of 2.66, 2.47 and 2.55 yielded a corresponding slope and R^2 equation to − 2.66 and 0.996 for the 24 h,
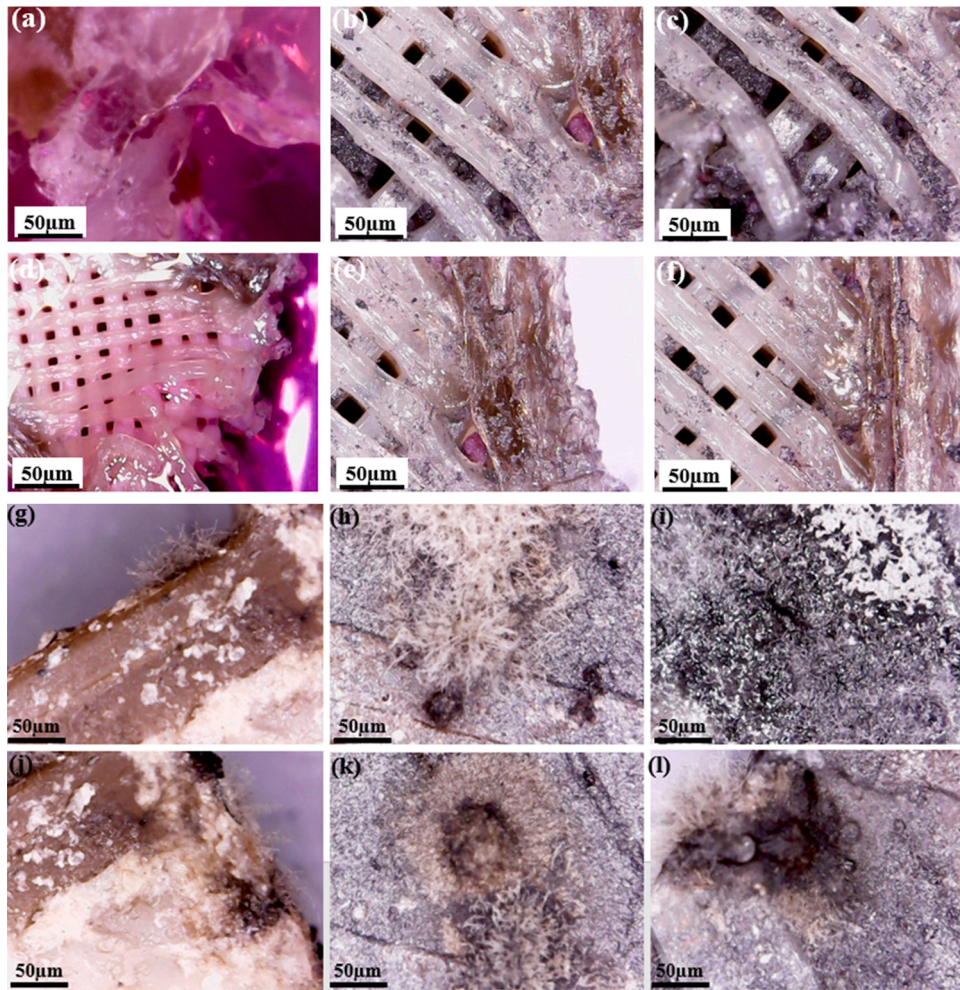
Fig. 6. Live/dead staining of cells attached to FDM 3D-printed PEEK composite sample surfaces after culturing with DMEM, showing 50 μm: (a-b) PEEK for 24 h, (c-d) PEEK-rGO for 24 h, (e-f) PEEK-rGO with growing live-cell and (f) more cell activity in the third day in PEEK. NAS, showing 50 μm: (g) PEEK cell seventh day, (h-i) PEEK-rGO seventh day, (j) PEEK cell spreading more in 14th day and (k-l) PEEK-rGO in 14th day.

− 2.47 0.998 for the third day and − 2.55 and 0.997 for the seventh day. Fig. 5 shows the results of the PEEK-HAp with the Gaussian filter at a roughness amplitude of 0.80 mm for; (a) the texture direction of the converted luminance analysis of the PEEK nanoparticle, (b) scatter plot of the Sq height parameter of the nanoparticle in ISO25178 standard of PEEK-HAp and (c) failure analysis of the microstructure.

Fig. 6 shows the dynamics of the change of the scaffold with time after applying energy to the form of particle. It shows the computation 4D view of the five structures after the growth of the scaffold cell. The profiling of the scaffold in Fig. 6 indicates that the composite tested with NAS on the first day has the optimum surface profiling due to the slight change with time, but it shows a bit of cell growth.

4.3. In-vitro cytotoxicity results

Fig. 6 depicts the live/dead staining of cells attached to FDM 3D-printed PEEK composite sample surfaces after culturing with Dulbecco's modified eagle medium (DMEM), showing 50 μm: (a-b) PEEK for 24 h, (c-d) PEEK-rGO for 24 h, (e-f) PEEK-rGO with growing live-cell and (f) more cell activity in the third day in PEEK. Moreover, the Live/dead staining of cells attached to FDM 3D-printed PEEK composite sample surfaces after culturing with NAS showed 50 μm: (a) PEEK for 24 h, (b) PEEK-rGO for 24 h, (c) PEEK-rGO with growing live-cell, (d) more cell activity in the third day in PEEK, (e) PEEK-rGO in the third day, (f) cell growing more on PEEK-rGO, (g) PEEK cell spreading with

tiny dead cell in the seventh day, (h-i) PEEK-rGO cell growing and spreading with small dead cell in the seventh day, (j) PEEK cell spreading more in 14th day and (k-l) PEEK-rGO with a dead cell in 14th day.

As biomedical/bone tissue engineering requires, the composite scaffolds can be suitable alternatives for biomimetic heterogeneous artificial bone repair. It showed that with the increment of the porosity, the difference between the theoretical porosity and the calculated results via CAD modelling also increased, but the error was 5%. This result significantly implied that the established porosity calculation model could effectively predict the porosity size of the structure. It can be observed that the 2 wt% composite was the optimum scaffold to be considered.

5. Conclusions

The excellent mechanical properties and high aspect rate of rGO have attracted great potential. The effects of rGO on the PEEK composite-epoxy matrix have been analysed in this study. The following significant concluding remarks can be deduced from the investigation:

- PEEK-rGO composite scaffolds with interconnected pore lattices were possibly 3D-printed through AM technology.
- The major novelty included the scaffold production of PEEK-rGO with ratios of 1–3% for an implant, combining a different lattice

with PEEK and rGO for a bone implant. The optimum or best composite ratio and excellent mechanical strength were obtained at 3 wt % of rGO.

- The composite tensile strength, stiffness and Young's modulus increased compared with the pure epoxy matrix with 1 and 2 wt% of rGO. Their tensile strengths decreased when the percentage of the polymer increased. 3D printing of novel bioactive scaffolds of PEEK incorporating rGO can enable the fabrication of custom-made shaped scaffolds.
- Possibility of effective mechanical testing, data analysis and cell culture tests for in-vitro biocompatibility scaffold characterisation for the PEEK composites.
- Novel computation microanalysis of 4D printing of microstructure of PEEK-rGO concerning the grain size and 3D morphology was influenced by furrow segmentation of grains cell growth on the composite, which was reduced from an average of 216–155 grains and increased to 253 grains on the last day.

Ethical statement

The authors declare no ethical issue; the study was conducted entirely with ethical standards. Also, the manuscript is neither under review nor published elsewhere.

CRediT authorship contribution statement

Bankole I. Oladapo: Conceptualisation, Methodology, Software, Writing – original draft. Validation, Visualisation, Investigation, Writing – review & editing, Funding acquisition, Resources. **Sikiru O. Ismail:** Project administration, Validation, Writing – review & editing, Supervision, Writing – review & editing, Data curation. **Omolayo M. Ikumapayi:** Supervision, Validation, Visualisation, Writing – review & editing, Funding acquisition. **Panagiotis G. Karagiannidis:** Writing-review & editing, Supervision, Investigation, Project administration.

Declaration of Competing Interest

The authors declare that they have no known competing for financial interests or personal relationships that could have appeared to influence the work reported in this paper.

Acknowledgment

None.

References

[1] B.I. Oladapo, S.A. Zahedi, Improving bioactivity and strength of PEEK composite polymer for bone application, Mater. Chem. Phys. 266 (2021), 124485, https://doi.org/10.1016/j.matchemphys.2021.124485.
[2] G. Nyiranzeyimana, J.M. Mutua, B.R. Mose, T.O. Mbuya, Optimization of process parameters in fused deposition modelling of thermoplastics: a review, Mater. Werkst. 52 (2021) 682–694, https://doi.org/10.1002/mawe.202000193.
[3] C.P. Khunt, M.A. Makhesana, B.K. Mawandiya, K.M. Patel, Investigations on the influence of printing parameters during processing of biocompatible polymer in Fused Deposition Modelling (FDM) (ahead-of-print), Adv. Mater. Process Technol. Abingdon Engl. (2021) 1–17, https://doi.org/10.1080/2374068X.2021.1927651.
[4] F. Alam, K.M. Varadarajan, J.H. Koo, B.L. Wardle, S. Kumar, Additively manufactured polyetheretherketone (PEEK) with carbon nanostructure reinforcement for biomedical structural applications, 2000483-n/a, Adv. Eng. Mater. 22 (2020), https://doi.org/10.1002/adem.202000483.
[5] D. Almasi, N. Iqbal, M. Sadeghi, I. Sudin, M.R. Abdul Kadir, T. Kamarul, Preparation methods for improving PEEK's bioactivity for orthopedic and dental application: a review, Int. J. Biomater. 2016 (2016), e8202653, https://doi.org/10.1155/2016/8202653.
[6] B.I. Oladapo, S.A. Zahedi, S.O. Ismail, F.T. Omigbodun, 3D printing of PEEK and its composite to increase biointerfaces as a biomedical material- a review, Colloids Surf. B Biointerfaces 203 (2021), 111726, https://doi.org/10.1016/j.colsurfb.2021.111726.
[7] M.S. Kang, S.J. Jeong, S.H. Lee, B. Kim, S.W. Hong, J.H. Lee, et al., Reduced graphene oxide coating enhances osteogenic differentiation of human mesenchymal stem cells on Ti surfaces, Biomater. Res 25 (2021) 4, https://doi.org/10.1186/s40824-021-00205-x.
[8] S. Bahrami, N. Baheiraei, M. Shahrezaee, Biomimetic reduced graphene oxide coated collagen scaffold for in situ bone regeneration, Sci. Rep. 11 (2021) 16783, https://doi.org/10.1038/s41598-021-96271-1.
[9] M. Ahamed, M.J. Akhtar, M.A.M. Khan, H.A. Alhadlaq, A novel green preparation of Ag/RGO nanocomposites with highly effective anticancer performance, Polymers 13 (2021) 3350, https://doi.org/10.3390/polym13193350.
[10] M. Ahamed, M.J. Akhtar, M.M. Khan, H.A. Alhadlaq, SnO2-doped ZnO/reduced graphene oxide nanocomposites: synthesis, characterization, and improved anticancer activity via oxidative stress pathway, Int. J. Nanomed. 16 (2021) 89–104, https://doi.org/10.2147/IJN.S285392.
[11] J. Cheng, J. Liu, B. Wu, Z. Liu, M. Li, X. Wang, P. Tang, Z. Wang, Graphene and its derivatives for bone tissue engineering: in vitro and in vivo evaluation of graphene-based scaffolds, membranes and coatings, Front. Bioeng. Biotechnol. 9 (2021) 9.
[12] A.T. Smith, A.M. LaChance, S. Zeng, B. Liu, L. Sun, Synthesis, properties, and applications of graphene oxide/reduced graphene oxide and their nanocomposites, Nano Mater. Sci. 1 (2019) 31–47.
[13] S. Wang, N. Liu, J. Su, L. Li, F. Long, Z. Zou, X. Jiang, Y. Gao, Highly stretchable and self-healable supercapacitor with reduced graphene oxide based fiber springs, ACS Nano 11 (2017) 2066–2074.
[14] M. Ahamed, M.J. Akhtar, M.A.M. Khan, H.A. Alhadlaq, Enhanced anticancer performance of eco-friendly-prepared Mo-ZnO/RGO nanocomposites: role of oxidative stress and apoptosis, ACS Omega 7 (2022) 7103–7115, https://doi.org/10.1021/acsomega.1c06789.
[15] J.C. Camargo, Á.R. Machado, E.C. Almeida, E.F.M.S. Silva, Mechanical properties of PLA-graphene filament for FDM 3D printing, Int. J. Adv. Manuf. Technol. 103 (2019) 2423–2443, https://doi.org/10.1007/s00170-019-03532-5.
[16] S. Barkarmo, A. Wennerberg, M. Hoffman, P. Kjellin, K. Breding, P. Handa, et al., Nano-hydroxyapatite-coated PEEK implants: A pilot study in rabbit bone, J. Biomed. Mater. Res. A 101A (2013) 465–471, https://doi.org/10.1002/jbm.a.34358.
[17] B.I. Oladapo, S.A. Zahedi, F.T. Omigbodun, A systematic review of polymer composite in biomedical engineering, Eur. Polym. J. 154 (2021) 110534, https://doi.org/10.1016/j.eurpolymj.2021.110534.
[18] B.I. Oladapo, S.A. Zahedi, S.O. Ismail, Mechanical performances of hip implant design and fabrication with PEEK composite, Polymer 227 (2021), 123865.
[19] B.I. Oladapo, S.A. Zahedi, S.O. Ismail, D.B. Olawade, Recent advances in biopolymer composite materials: Future sustainability of bone-implant, Renew. Sustain Energy Rev. 150 (2021), 111505, https://doi.org/10.1016/j.rser.2021.111505.
[20] J. Anguiano-Sanchez, O. Martinez-Romero, H.R. Siller, J.A. Diaz-Elizondo, E. Flores-Villalba, C.A. Rodriguez, Influence of PEEK coating on hip implant stress shielding: a finite element analysis, 6183679–10, Comput. Math. Methods Med. 2016 (2016), https://doi.org/10.1155/2016/6183679.
[21] B.I. Oladapo, S.O. Ismail, O.K. Bowoto, F.T. Omigbodun, M.A. Olawumi, M.A. Muhammad, Lattice design and 3D-printing of PEEK with Ca10(OH)(PO4)3 and in-vitro bio-composite for bone implant, Int. J. Biol. Macromol. 165 (2020) 50–62, https://doi.org/10.1016/j.ijbiomac.2020.09.175.
[22] B.I. Oladapo, S.O. Ismail, A.V. Adebiyi, F.T. Omigbodun, M.A. Olawumi, D.B. Olawade, Nanostructural interface and strength of polymer composite scaffolds applied to intervertebral bone, Colloids Surf. Physicochem Eng. Asp. (2021) 627, https://doi.org/10.1016/j.colsurfa.2021.127190.
[23] A.M.E. Arefin, N.R. Khatri, N. Kulkarni, P.F. Egan, Polymer 3D printing review: materials, process, and design strategies for medical applications, Polymers 13 (2021) 1499, https://doi.org/10.3390/polym13091499.
[24] B.I. Oladapo, S.A. Zahedi, S.O. Ismail, F.T. Omigbodun, O.K. Bowoto, M.A. Olawumi, et al., 3D printing of PEEK–cHAp scaffold for medical bone implant, Bio-Des. Manuf. 4 (2021) 44–59, https://doi.org/10.1007/s42242-020-00098-0.
[25] B.I. Oladapo, S.A. Zahedi, A.O.M. Adeoye, 3D printing of bone scaffolds with hybrid biomaterials, Compos Part B Eng. 158 (2019) 428–436, https://doi.org/10.1016/j.compositesb.2018.09.065.
[26] B.I. Oladapo, S.O. Ismail, M. Zahedi, A. Khan, H. Usman, 3D printing and morphological characterisation of polymeric composite scaffolds, Eng. Struct. 216 (2020), 110752, https://doi.org/10.1016/j.engstruct.2020.110752.
[27] B.I. Oladapo, A.O.M. Adeoye, M. Ismail, Analytical optimization of a nanoparticle of microstructural fused deposition of resins for additive manufacturing, Compos Part B Eng. 150 (2018) 248–254, https://doi.org/10.1016/j.compositesb.2018.05.041.
[28] B.I. Oladapo, I.A. Daniyan, O.M. Ikumapayi, O.B. Malachi, I.O. Malachi, Microanalysis of hybrid characterization of PLA/cHA polymer scaffolds for bone regeneration, Polym. Test. 83 (2020) 106341, https://doi.org/10.1016/j.polymertesting.2020.106341.
[29] Y.-W. Du, L.-N. Zhang, X. Ye, H.-M. Nie, Z.-T. Hou, T.-H. Zeng, et al., In vitro and in vivo evaluation of bone morphogenetic protein-2 (BMP-2) immobilized collagen-coated polyetheretherketone (PEEK), Front Mater. Sci. 9 (2015) 38–50, https://doi.org/10.1007/s11706-015-0276-x.
[30] M. Grau, J. Matena, M. Teske, S. Petersen, P. Aliuos, L. Roland, et al., In vitro evaluation of PCL and P(3HB) as coating, Mater. Sel. Laser Melted Porous Titan. Implants Mater. 10 (2017) 1344, https://doi.org/10.3390/ma10121344.
[31] B.I. Oladapo, S.A. Zahedi, V.A. Balogun, S.O. Ismail, Y.A. Samad, Overview of additive manufacturing biopolymer composites, in: D. Brabazon (Ed.), Encycl. Mater. Compos., Elsevier, Oxford, 2021, pp. 915–928, https://doi.org/10.1016/B978-0-12-819724-0.00035-5.
[32] A. Merolli, L. Rocchi, M. De Spirito, F. Federico, A. Morini, L. Mingarelli, et al., Debris of carbon-fibers originated from a CFRP (pEEK) wrist-plate triggered a

destruent synovitis in human, J. Mater. Sci. Mater. Med 27 (2016) 1–10, https://doi.org/10.1007/s10856-015-5664-3.

[33] G.M. Vlăsceanu, H. Iovu, M. Ioniţă, Graphene inks for the 3D printing of cell culture scaffolds and related molecular arrays, Compos Part B Eng. 162 (2019) 712–723, https://doi.org/10.1016/j.compositesb.2019.01.010.

[34] B.I. Oladapo, E.A. Oshin, A.M. Olawumi, Nanostructural computation of 4D printing carboxymethylcellulose (CMC) composite, Nano-Struct. Nano-Objects 21 (2020), 100423.

[35] H.Y. Jeong, E. Lee, S.-C. An, Y. Lim, Y.C. Jun, 3D and 4D printing for optics and metaphotonics, Nanophotonics 9 (2020) 1139–1160.

[36] J. Xiong, R. Mines, R. Ghosh, A. Vaziri, L. Ma, A. Ohrndorf, et al., Advanced micro-lattice materials, Adv. Eng. Mater. 17 (2015) 1253–1264, https://doi.org/10.1002/adem.201400471.

[37] O.P. Bodunde, O.M. Ikumapayi, E.T. Akinlabi, B.I. Oladapo, A.O.M. Adeoye, S.O. Fatoba, A futuristic insight into a "nano-doctor": A clinical review on medical diagnosis and devices using nanotechnology, Mater. Today Proc. 44 (2021) 1144–1153, https://doi.org/10.1016/j.matpr.2020.11.232.

[38] A.O.M. Adeoye, B.I. Oladapo, A.A. Adekunle, A.J. Olademeji, J.F. Kayode, Design, simulation and implementation of a PID vector control for EHVPMSM for an automobile with hybrid technology, J. Mater. Res. Technol. 8 (2019) 54–62, https://doi.org/10.1016/j.jmrt.2017.07.005.

[39] B.I. Oladapo, I.O. Malachi, O.B. Malachi, I.E. Elemure, A.M. Olawumi, Nanostructures of 4D morphology surface analysis of C1.7Mn0.6P0.1S0.07 (SAE 1045) tool wear, Nano-Struct. Nano-Objects 22 (2020), 100433, https://doi.org/10.1016/j.nanoso.2020.100433.

[40] BankoleI. Oladapo, S. Abolfazl Zahedi, F. Vahidnia, O.M. Ikumapayi, M.U. Farooq, Three-dimensional finite element analysis of a porcelain crowned tooth, Beni-Suef Univ. J. Basic Appl. Sci. 7 (2018) 461–464, https://doi.org/10.1016/j.bjbas.2018.04.002.

[41] X. Shi, B. Chen, X. Tuo, Y. Gong, J. Guo, Study on performance characteristics of fused deposition modeling 3D-printed composites by blending and lamination, 32495-n/a, J. Appl. Polym. Sci. 138 (2021), https://doi.org/10.1002/app.49926.

[42] A. Kehinde Aworinde, S. Oluropo Adeosun, F. Adekunle Oyawale, E. Titilayo Akinlabi, S.A. Akinlabi, Parametric effects of fused deposition modelling on the mechanical properties of polylactide composites: a review, J. Phys. Conf. Ser. 1378 (2019) 22060, https://doi.org/10.1088/1742-6596/1378/2/022060.